View Online / Journal Homepage / Table of Contents for this issue
Dynamic Article Links

Soft Matter

Cite this: *Soft Matter*, 2012, **8**, 10032

www.rsc.org/softmatter

PAPER

Measuring the elastic modulus of microgels using microdrops

Adam R. Abate,*[abc] Lloyd Han,[ab] Lihua Jin,[b] Zhigang Suo[b] and David A. Weitz[ab]

Received 13th May 2012, Accepted 30th July 2012
DOI: 10.1039/c2sm26108a

Two microgel particles are encapsulated in a microdrop having a spherical diameter smaller than the sum of the diameters of the microgels; this causes the microgels to be squeezed together by the oil–water interface of the drop, in turn, making the drop ellipsoidal in shape. By modeling the force applied to the microgels by the drop and equating this to the Hertz contact force of their deformation, we are able to estimate their elastic modulus. By varying the surface tension and shape of the drops, we are able to measure the modulus of the microgels under different loads. This provides a simple technique for quantifying the elasticity of small, deformable objects, including liquid drops, microgels, and cells.

Introduction

Many systems of importance in biological, chemical, and physical research are composed of micro-scale objects that are deformable. The tissues of organisms, for instance, are composed of cells embedded in extracellular matrix, where the cell elasticity imparts important mechanical properties to the tissues.[1–3] Complex materials like colloidal suspensions, emulsions, and foams, are important for chemical and physical studies; they are composed of deformable objects, including microgels, drops, or bubbles, the elastic properties of which can influence the flow and function of the material.[4–8] To quantify the properties of important systems like these, it is critical to accurately understand the properties of the individual objects of which they are composed.

Atomic Force Microscopy (AFM) can be used to measure the elastic properties of small objects through microindentation: The AFM tip is pressed into the object with a controlled force, and by measuring the deformation of the object, the elastic modulus can be estimated.[9–11] One challenge of this approach, however, is that the object must be adhered to a surface; this can pre-stress the object, perturbing its modulus. A less perturbative approach is to use capillary micromechanics, in which the object is forced through a tapered capillary; by measuring the shape-deformation of the object as it moves through the capillary, its elastic properties can be estimated.[12] Like AFM, however, this approach requires specialized equipment and also that each object be probed individually; this is often done using manual manipulation, adding tedious and timing consuming steps to the process that limit the number of objects that can be characterized. To enable simpler, more accurate characterization of larger numbers of objects, new methods are needed.

In this paper, we introduce a technique to measure the elastic properties of microscopic objects; the technique is simple, requires only a brightfield microscope for droplet imaging, and can easily be used to characterize large number of objects to obtain elastic modulus measurements with high statistical certainty. In our technique, the interface of a microdrop is used to apply controlled forces to microgels encapsulated in the microdrop. By modeling the forces applied to the microgel by the droplet interface and equating these to the elastic response of the microgels, we are able to estimate the elastic modulus.

Materials and methods

We present a general methodology that can be used to measure the elasticity of microscopic deformable objects. The methodology does not require microfluidic devices, only chemicals with which to form an emulsion, and a microscope with which to image the resultant particle-containing droplets. However, for the data we present below, we used particles that were synthesized using microfluidics, although the same measurement methodology can be applied to particles synthesized using other non-microfluidic techniques, such as emulsion polymerization.

Fabrication of microfluidic devices

We use microfluidic devices to synthesize microgel particles and to image them after they have been encapsulated in drops. The microgel synthesis device consists of a cross-junction drop maker[13,14] with dimensions 25 μm in width and height. The imaging device consists of a channel 700 μm in width and 100 μm in height. Both are fabricated in poly(dimethylsiloxane) using the techniques of soft lithography.[15] The devices are functionalized with a hydrophobic treatment (Aquapel™) to ensure that the drops do not wet the channel walls. To functionalize the devices, ~50 μL of Aquapel is flushed into the channels and the channels

[a]*Department of Physics, Harvard University, Cambridge, Massachusetts 02138, USA. E-mail: adam.abate@ucsf.edu*
[b]*School of Engineering and Applied Sciences and Kavli Institute for Nanobio Science and Technology, Harvard University, Cambridge, Massachusetts 02138, USA*
[c]*Department of Bioengineering and Therapeutic Sciences, University of California, San Francisco, California 94158, USA*

are blown dry with air. The devices are baked at 65 °C for 1 h before use.

Synthesis of monodisperse microgels

The microgels are synthesized using a microfluidic drop maker to form an emulsion consisting of drops of acrylamide (6.5 vol%), bis-acrylamide (9 vol%), and adenosine 5′-phosphosulfate sodium (2 vol%), aqueous. The carrier oil consists of HFE-7500 with the ammonium carboxylate of Krytox FSL (2 wt%) as surfactant, and tetramethylethylenediamine (TEMED) as a polymerization accelerant (0.4 vol%). The newly formed drops are collected into a clean glass vial and heated to 65 °C for 12 h in an oven. During this time, TEMED from the oil diffuses into the drops, accelerating polymerization and crosslinking of the monomers, and gelling the drops. The polymer and crosslinking concentrations of the resultant microgels can be tuned by varying the concentrations of the precursors. After the gels have solidified, they are re-dispersed into water. We add 1 mL of 20% perfluorooctanol in HFE-7500 to the emulsion and vortexed and centrifuged the mixture at 5000 rpm for 30 s. The lower oil phase is removed with a pipette and 1 mL of 1% span80 in hexane is added, and the mixture vortexed and centrifuged again. The upper hexane layer is pipetted off, an additional 1 mL of hexane is added, and the process is repeated once more. The hexane is again removed and 1 mL of water is added to re-disperse the microgels.

Encapsulation of microgels in drops

To encapsulate microgels in drops, oil and surfactant is added to the microgel suspension and the mixture is shaken to generate an emulsion. To achieve greater control over the number of microgels encapsulated in the drops, valve-based flow focusing combined with close-packed encapsulation can be used.[16,17] We use two oil and surfactant formulations. To enable confocal imaging of microgel-containing drops (Fig. 1A), we use Krytox GPL 100, which has an index of refraction similar to that of water; this lowers refraction through the drop interface, allowing confocal visualization of its interior. To dye the middle phase of the drop, we use a solution of fluorescently labeled bovine serum albumin (BSA) at 10^{-6} wt%. Because the dye molecules are attached to bulky BSA proteins, they are prevented from diffusing into the microgels because the hydrodynamic diameter of the proteins they are tethered to is larger than the microgel pore size. This confines the dye molecules to the aqueous phase of the droplet, so that the edges of the oil–water interface and microgel particles can be clearly imaged, as shown in Fig. 1A. This allows us to clearly image the microgel and droplet surfaces, which are used to model the forces. To stabilize these drops, we use the Krytox FSL surfactant at 2 wt%, yielding a surface tension of ~4 mN m^{-1}. To enable brightfield imaging of the drops (Fig. 2), we use mineral oil with the surfactant ABIL EM 90 at different concentrations. We measure the surface tensions of these emulsions individually using a tensiometer, and use these values for the calculations that follow.

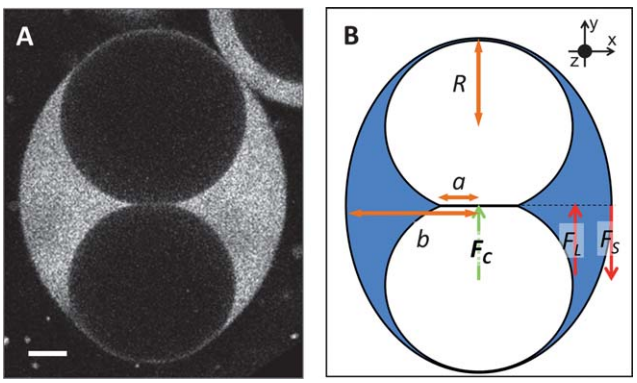

Fig. 1 Confocal microscope image of two microgels (dark circles) squeezed together by the interface of a fluorescent droplet, (A). The scale bar denotes 10 μm. (B) Force diagram for microgel-containing drops: F_S is the surface tension force, F_L the Laplace pressure force, and F_C the contact force of the microgels. F_C and F_L denote compressive forces, while F_S denotes a tensile force.

Imaging microgel-containing drops

Because the emulsions are formed with shaking, they contain drops of a wide range of sizes encapsulating different numbers of microgels. Some of these drops, purely by chance, will contain exactly two microgels in the configuration needed for force modeling. To image these rare drops, we search the emulsion by flowing it through the large channel described above. This is accomplished by loaded the emulsion into a syringe and injecting it into the channel *via* a tube. We image the drops as they flow through the channel. When a drop containing two microgels is

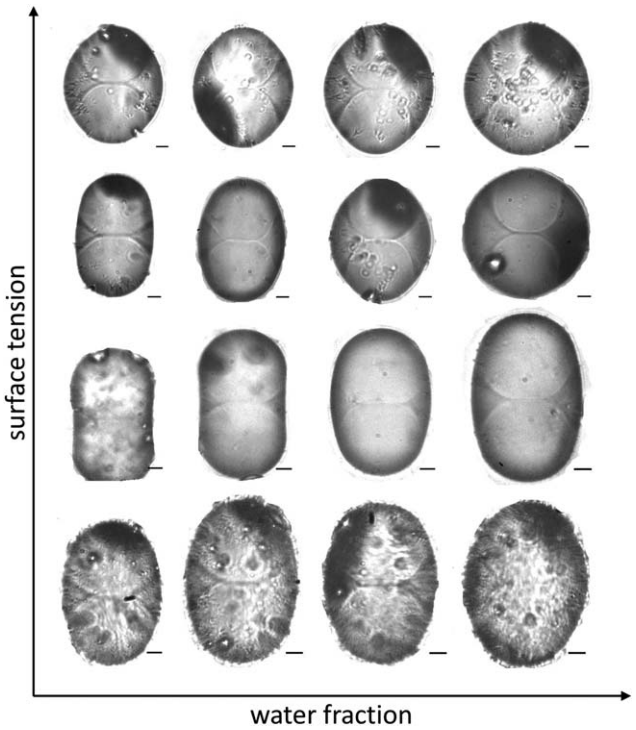

Fig. 2 Brightfield microscopy images of microgel-containing droplets for different surface tension and water volume fractions. Each droplet contains two microgels squeezed together by the droplet interface. The scale bars denote 10 μm.

detected, we stop the flow and record an image. After the image is recorded, the flow is re-started to search for another microgel-containing drop. Using this simple technique, we image ~50 drops in ~10 minutes, each of which provides one measurement of the microgel modulus.

Results and discussion

Modeling the forces of microgel-containing drops

When two microgels are encapsulated in a drop having a spherical diameter smaller than the sum of the diameters of the microgels, the drop is ellipsoidal in shape. The ellipsoidal drop has a higher surface area than a sphere of equivalent volume, causing the interface to squeeze inward on the microgels, as shown in Fig. 1A. Shortly after the microgels are encapsulated in the drop, the system achieves mechanical equilibrium. Defining a Cartesian coordinate system with an origin at the geometrical center of the drop, force balance for the xz plane at $y = 0$ dictates that

$$F_C = F_S - F_L, \quad (1)$$

where F_C is the contact force of the microgels,

$$F_S = 2\pi b\gamma \quad (2)$$

is the surface tension force, and

$$F_L = \Delta p\pi(b^2 - a^2) \quad (3)$$

is the Laplace pressure force; b is the radius of curvature of the drop in the xz plane that is positioned at $y = 0$ (Fig. 1B), γ the oil–water interfacial tension, Δp the pressure difference across the water–oil interface, and a the contact radius of the microgels. We can measure b and a directly from the images, while Δp can be calculated from the Young–Laplace equation,

$$\Delta p = \gamma(1/R_b + 1/b) \quad (4)$$

with R_b the radius of curvature of the drop interface in the xy plane that is positioned at $z = 0$. For moderate deformations of the microgels, the elastic response can be modeled according to Hertz contact,

$$F_C = 4Ea^3/[3R\,(1 - \nu)^2], \quad (5)$$

where R is the effective radius of the particles defined as $1/R = 1/R_1 + 1/R_2$, with R_1 and R_2 the respective radii of the particles in the drop; E is the elastic modulus of the microgels and ν is the Poisson ratio, which we set equal to 0.5. By combining eqn (1)–(5), we obtain an expression for the elastic modulus that depends only on known or measureable parameters,

$$E = 3\pi R\gamma(1 - \nu)^2(2b - (b^2 - a^2)(1/R_b + 1/b))/4a^3. \quad (6)$$

Measuring E under different applied loads

Our technique can be used to obtain a force-dependent measurement of the microgel modulus. To do this, we measure the microgel modulus for different compression forces, which correspond to different equilibrium states of the drops. From dimensional analyses, we determine that two dimensionless groups govern the equilibrium states of the drops, γ/ER and V/R^3, where V is the volume of water encapsulated in the drop with the microgels; by varying the surface tensions and water volume fractions f_w of the drops, with $f_w = V/V_d$ and V_d the total droplet volume, we are thus able to apply different compression forces to the microgels.

To vary surface tensions, we change the concentration of surfactant in the middle phase. To vary shapes and water volume fractions, we create the drops by shaking, which naturally forms drops over a range of shapes. Sample images of drops from our emulsions are shown ordered according to increasing surface tension and water volume fraction (more spherical shapes) in Fig. 2.

To estimate the modulus of the microgels from the images, we calculate the values of F_S, F_L, and F_C for each drop. The force F_S scaled by γR is plotted as a function of f_w in Fig. 3A. The data for different surfactant concentrations collapse to a line that

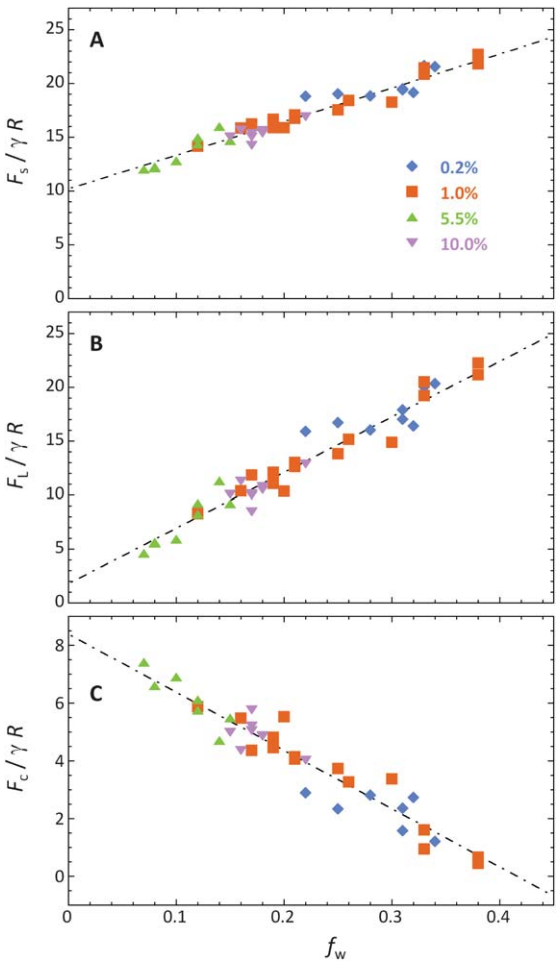

Fig. 3 Forces in microgel-containing drops as a function of the water volume fraction of the drop, which is related to its shape—larger water volume fraction correspond to drops that are more spherical in shape. (A) Surface tension force, (B) Laplace pressure force, and (C) contact force applied to the microgels, $F_C = F_S - F_L$. The legend in (A) indicates surfactant concentrations.

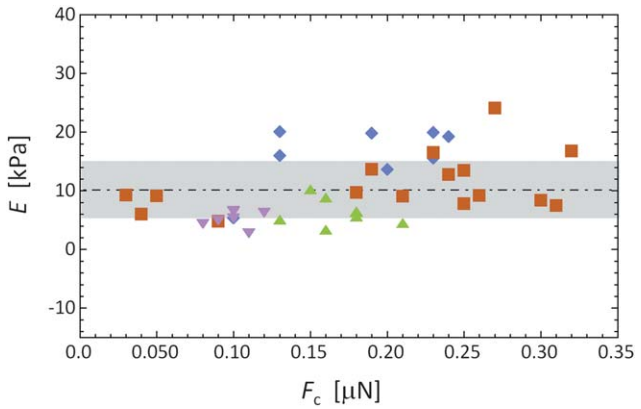

Fig. 4 Microgel elastic modulus *versus* compression force $F_C = F_S - F_L$. The data have an average value of 10.2 ± 5.5 kPa, as indicated by the dashed line; the grayed area represents the error in the measurement. This value is consistent with polyacrylamide gels for our monomer and crosslinker concentrations.

increases with f_w, since this produces more spherical drops. Opposing this is the Laplace pressure force of the drop F_L, which is also scaled by γR and plotted as a function of f_w in Fig. 3B. The Laplace force data also collapse to a line that increases with f_w. The net force applied to the microgels, $F_C = F_S - F_L$, scaled by γR is plotted against f_w in Fig. 3C. Even though F_S and F_L increase with f_w, their difference, corresponding to the compression force applied to the microgels, decreases; this is because the Laplace pressure force increases more rapidly than the surface tension force as the drops become more spherical, as can be seen by comparing the slopes of the lines in Fig. 3A and B.

To complete our estimation of the microgel modulus, we equate the net force $F_S - F_L$ to the Hertz contact force of the microgels and solve for the elastic modulus (eqn (6)). For every drop we observe, we use this equation to obtain an estimate of E and plot the results as a function of the compression force F_C in Fig. 4. While the data are noisy, we obtain an average value of 10.2 ± 5.5 kPa for our microgels, which is consistent with the modulus of bulk polyacrylamide gels for our monomer and crosslinker concentrations. The error in the measurement is due, primarily, to error in measuring a, since F_C depends on the cube of this value. Our method can thus correctly measure the elastic modulus of microgels composed of a known material. While there is a very slight upward trend in our data, for the loads tested the modulus is essentially constant within the measurement error; for smaller drops and larger interfacial tensions, it would be possible to apply larger loads and potentially observe E to increase with F_C, which would be expected for non-linear response of the microgels.

Conclusions

We have presented a simple technique to measure the elasticity of microscopic objects. In contrast to conventional approaches like atomic force microscopy or microcapillary aspiration, our droplet technique requires only a brightfield microscope for droplet imaging and can be used to characterize objects of a wide range of sizes and elasticities. It also affords an unperturbed measurement of the object's elastic properties and allows large numbers of objects to be analyzed easily, providing elastic modulus estimates with a high degree of statistical certainty. It can be used to characterize objects having a modulus close to the capillary pressure of the drops, making it useful for most cells, liquid drops, and microgels, including hydrogels and oleophilic gels.

Acknowledgements

We thank Louise Jawerth for her help with the confocal imaging. This work was supported by the BASF, Advanced Research Initiative at Harvard University, and by the NSF (grant DMR-1006546), and the MRSEC (grant DMR-082084). L.J. and Z.S. are supported by MURI through a contract on Adaptive Structural Materials (W911NF-09-1-0476).

References

1 V. H. Barocas and R. T. Tranquillo, An anisotropic biphasic theory of tissue-equivalent mechanics: the interplay among cell traction, fibrillar network deformation, fibril alignment, and cell contact guidance, *J. Biomech. Eng.*, 1997, **119**, 137–145.
2 K. E. Kasza, *et al.*, The cell as a material, *Curr. Opin. Cell Biol.*, 2007, **19**, 101–107, DOI: 10.1016/j.ceb.2006.12.002.
3 T. Wakatsuki, M. S. Kolodney, G. I. Zahalak and E. L. Elson. Cell mechanics studied by a reconstituted model tissue. *Biophys. J.* 2000, **79**, 2353–2368.
4 W. B. Russel, Review of the role of colloidal forces in the rheology of suspensions, *J. Rheol.*, 1980, **24**, 287–317.
5 H. A. Barnes, Rheology of emulsions — a review, *Colloids Surf., A*, 1994, **91**, 89–95.
6 D. J. Durian, Foam mechanics at the bubble scale, *Phys. Rev. Lett.*, 1995, **75**, 4780–4783.
7 P. Sollich, F. Lequeux, P. Hebraud and M. E. Cates, Rheology of soft glassy materials, *Phys. Rev. Lett.*, 1997, **78**, 2020–2023.
8 S. M. Fielding, P. Sollich and M. E. Cates, Aging and rheology in soft materials, *J. Rheol.*, 2000, **44**, 323–369.
9 W. H. Goldmann and R. M. Ezzell, Viscoelasticity in wild-type and vinculin-deficient (5.51) mouse F9 embryonic carcinoma cells examined by atomic force microscopy and rheology, *Exp. Cell Res.*, 1996, **226**, 234–237.
10 A. Vinckier and G. Semenza, Measuring elasticity of biological materials by atomic force microscopy, *FEBS Lett.*, 1998, **430**, 12–16.
11 J. L. Alonso and W. H. Goldmann, Feeling the forces: atomic force microscopy in cell biology, *Life Sci.*, 2003, **72**, 2553–2560, DOI: 10.1016/S0024-3205(03)00165-6.
12 H. M. Wyss, *et al.*, Biophysical properties of normal and diseased renal glomeruli, *Am. J. Physiol.: Cell Physiol.*, 2010, C490–C498, DOI: 10.1152/ajpcell.00438.2010.
13 S. L. Anna, N. Bontoux and H. A. Stone, Formation of dispersions using "flow focusing" in microchannels, *Appl. Phys. Lett.*, 2003, **82**, 364–366, DOI: 10.1063/1.1537519.
14 A. R. Abate, *et al.*, Impact of inlet channel geometry on microfluidic drop formation, *Phys. Rev. E: Stat., Nonlinear, Soft Matter Phys.*, 2009, **80**, 026310, DOI: 10.1103/Physreve.80.026310.
15 Y. N. Xia and G. M. Whitesides, Soft lithography, *Abstr. Pap. Am. Chem. Soc.*, 1997, **214**, 348.
16 A. R. Abate, M. B. Romanowsky, J. J. Agresti and D. A. Weitz, Valve-based flow focusing for drop formation, *Appl. Phys. Lett.*, 2009, **94**, 023503, DOI: 10.1063/1.3067862.
17 A. R. Abate, C. H. Chen, J. J. Agresti and D. A. Weitz, Beating Poisson encapsulation statistics using close-packed ordering, *Lab Chip*, 2009, **9**, 2628–2631, DOI: 10.1039/B909386a.